

A Comparative study of pulsed and non-pulsed current on aspect ratio of weld bead and microstructure characteristics of AISI 304L stainless steel

Adnan A. Uгла

Department of Mechanical Engineering, Faculty of Engineering, University of Thi-Qar, Al-Nasiriyah, Iraq.

Abstract

The aim of this work is to investigate the influence of the welding process parameters on the weld bead geometry, microstructure characteristics, and mechanical properties of weldments carried out using TIG welding with pulsed/non pulsed current processes. The cooling state was introduced as an input parameter to investigate the main effects on the structure morphology and thereby the mechanical property. In this work the selected pulse frequency levels were 5-500 Hz in order to show the effect of low and high frequencies on the weldment characteristics of AISI 304L plates using filler metal of ER 308LSi. In this work, three levels four factors Taguchi L9 orthogonal array was used to analyze the aspect ratio of the welded specimens. Taguchi analysis was performed for the main effects plot to optimize the process parameters. Furthermore, the microstructure evolution has been investigated. Thus key findings of this work clarified that the pulse frequency has significant effect on the breaking of the dendrite arms during welding process and so strongly affects on the tensile strength. The cooling state also affects on the microstructure texture and thereby, the mechanical properties. The most important factor affects the bead geometry and aspect ratio is the travel speed.

Keywords: TIG welding, microstructure, mechanical properties, pulse frequency, austenitic stainless steel.

1. Introduction

Tungsten inert gas (TIG) welding is the most widely used process for joining the stainless steel components with thickness less 10 mm (Hamjah, 2014). It is very suitable for thin sheets due to its easier applicability, flexibility, and better economy (Mao et al, 2014). The improving in the weld quality depends on the improvement in process parameters which requires the use of improved welding techniques and materials. Pulsed current TIG welding (PCTW) is a variation of continuous current TIG welding (CCTW) where involves cycling the welding current at a given regular frequency from a high level to low level as describe by Namjou and others (2014). In PCTW process, the peak current (I_p) is selected to melt the filler and base metal and to generate adequate penetration, whereas the base current (I_b) is set at a level sufficient to maintain a stable arc (Yousefieh et al, 2011). By contrast, in CCTW, the heat required to melt the filler and base metals is supplied only during I_p pulses allowing the heat to dissipate into the base material (Balasubramanian et al, 2006). Devendranath Ramkumar and others (2015) used the pulsed and conventional TIG welding to study the weldability of AISI 904L stainless steel. They demonstrated that the PCTW generally offers better tensile properties as compared to CCTW weldments. Prasad and others (2012) used pulsed current in micro plasma arc welding process to study the quality of different types of stainless steels. They concluded that the AISI 304L achieved the better quality characteristics as comparison of AISI 316L, AISI 316Ti, and AISI 321. Dinesh Kumar et al. (2014) used Taguchi method to analysis and optimize the process parameters for pulsed TIG welding process of AISI 304L stainless steels. They showed that travel speed and current are the most important parameters which affect the response variables.

From the observation made on the above online literature, various properties of austenitic stainless steel weldments were investigation. The present work is an experimental investigation describes in detail the effects of pulse frequency and cooling state on the weld bead aspect ratio, microstructure, texture, and mechanical properties of TIG weldments using AISI 304L austenitic stainless steel. The overall purpose of this paper is to investigate:

1. The aspect ratio of the weld bead profile of Type 304L austenitic stainless steel components welded using conventional CCTW and pulsed current PCTW processes.
2. The morphology aspects and microstructure characteristics for Type 304L austenitic stainless steel components welded using conventional CCTW method and those welded using the pulsed current.
3. The mechanical properties such as tensile strength and ductility % of the fabricated components and their correlation with the resulted microstructure.

2. Materials and Research Method

The AISI 304L stainless steel is used in some of important industries such as containers of transporting chemicals, oil refinery, nuclear reactor tanks, dairy industries, and textile industries. In this work a 3.8 mm thick of similar 304L sheets has been welded by TIG technique. The filler metal selected for welding was ER 308LSi stainless steel solid wire with a diameter of 0.8 mm. The suggested shielding gas was Argon with 99.90% purity with 12 l/min. The 304L stainless steel plate and the welding metal were chemically analyzed, and the results of the analysis were listed in Table 1. The plates were cut using power hacksaw cutting machine. For bead on plate experiments, the required plate dimensions were (100 mm x 200 mm). Whereas for square butt joint configuration the required plate dimensions were (100 mm x 50 mm). The prepared parts were joined by CCTIG and PCTIG processes using LINCOLN TIG machine which can be used for continuous and pulsed currents. The pulsed current mode used in this welding machine shown in Figure 1. The joining process were done with/without filler metal and with/without using cooling system. The travel speed and arc length were controlled using CNC machine, whereas the wire feed rate controlled using external wire feed machine. The cooling water was with temperature of 20 °C and sufficient flow rate. Figure 2 shows the different units used in this work. In case of using cooling system, the 304L plates were placed on the copper backing plate, which was designed with internal water passages to increase the cooling rate of the melting pool zone (see Figure 2b). In order to measure the temperature during the welding process, the K Type thermocouple is the most suitable one (Sade ketal, 1995). The temperature was reading using an industrial data logger, which records the temperature at an interval of one second. To have defect free samples for testing, large number of trial runs were carried out with different combination of the process parameters. Some of process parameters were kept as constant during all experiments such as welding current of 175 A, peak time of 50%, background current of 87.5 A, arc length of 4 mm, wire feed angle of 40°, and stick out of 15 mm.

In this study, a four experimental factors three levels array was used for investigating the effects of process parameters on bead geometry. The range of each process parameter levels were selected based on trial welds and process parameters such as travel speed (TS), wire feed speed (WFS), pulse frequency (F), and introducing the cooling state (Cs) as a new factor as summarized in Table 2. For the purpose of optimization and obtaining the best possible results with the test number of experiments, the experiments were designed in the 'Minitab 17' software. Taguchi's L9 orthogonal array was used to design the experiments in the research work. In the L9 orthogonal array, nine experiments were prepared to study the effects of the main parameters. The nine experiments were carried out based on the L9 array and the nine specimens were welded using the different parameters and levels as shown in Table 3.

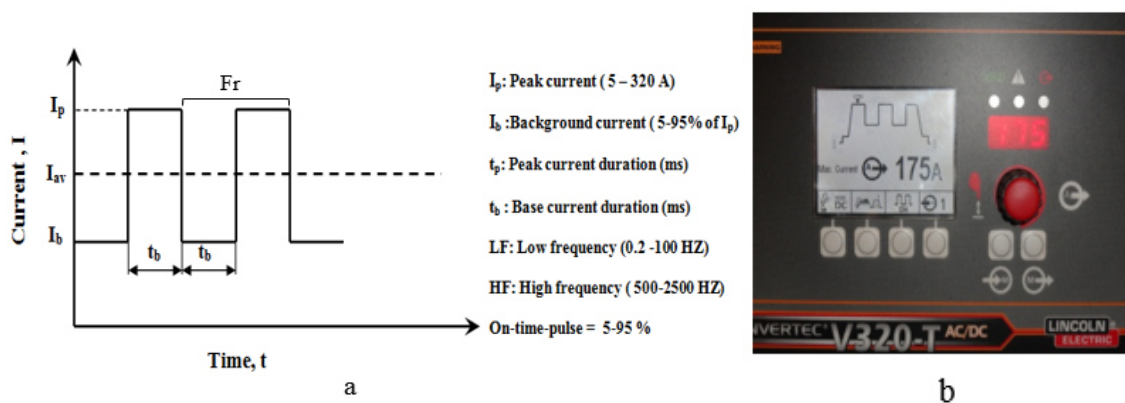


Figure 1 (a) Schematic diagram of a standard pulse current-time wave form in present PCSMD process and (b) picture illustrates the welding machine screen when it setup on the pulsed current state

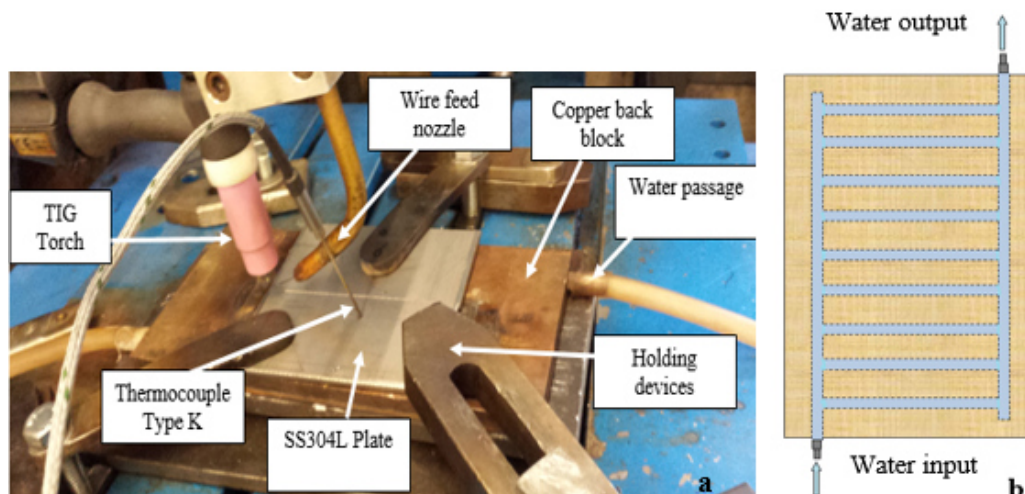


Figure 2 (a) TIG welding experimental setup and (b) schematic illustrates the water cooling system

Table 1 The chemical composition of the base and the filler materials (in wt.%)

Element	%C	%Si	%Mn	%S	%P	%Mo	%Ni	%Cr	%Fe	Others
SS304 actual composition	0.015	0.528	1.011	0.0107	0.02	0.053	8.202	18.164	Rem.	V = 0.10, Cu = 0.031 Ti = 0.01
ER308LSi as deposited composition	0.018	0.56	1.358	0.0331	0.033	0.115	9.412	19.557	Rem.	Co=0.941; Cu= 0.181 Ti=0.057

Table 2 Identified factors with levels

Symbol	Factor	Unit	Levels		
			1	2	3
TS	Travel speed	mm/s	1	2	3
WFS	Wire feed speed	m/minxp.	0	2	4
F	Pulse frequency	Hz	0	5	500
Cs	Cooling state	-----	0*	1**	2***

*No copper back strip; ** With copper back strip; *** With continuous water cooling system

Table 3 L9 control logTable with parameters and level values

Exp. No	TS	WFS	F	Cs
1	1	0	0	0
2	1	2	5	1
3	1	4	500	2
4	2	0	5	2
5	2	2	500	0
6	2	4	0	1
7	3	0	500	1
8	3	2	0	2
9	3	4	5	0

The weld bead profiles of all specimens were measured carefully and the observed values for bead width and depth of penetration with their aspect ratios and corresponding S/N ratios summarized in Table 4. In Taguchi method, the optimum value is obtained by calculating the signal to noise ratio. The term “signal” represents the desirable mean value, and the “noise” represents the undesirable value. Hence, the S/N ratio represents the amount of variation. S/N is the performance characteristic having three types such as (1) Higher the better, (2) lower the better, and (3) nominal the better. In the current work, the weld bead characteristics such as depth of the penetration and bead width of the tested weld specimens were identified as the response. The depth of penetration is considered as required sign and bead width is considered as undesirable sign therefore the aspect ratio (W/P) is considered as smaller the better (SB) is used for minimizing the aspect ratio of the welded parts. The smaller the better performance is expressed

$$S/N_{SB} = -10 \log \left[\frac{1}{n} \sum_{i=1}^n y_i^2 \right] \quad (1)$$

where n is the number of repetition of output response in the same trial and y is the response.

Table 4 Taguchi L9 orthogonal array and experimental results of the responses

Exp. No	Observations of bead width (mm)			Mean W (mm)	Observation of penetration (mm)			Mean P (mm)	Aspect ratio	S/N values of aspect ratio
	1	2	3		1	2	3			
1	16.5	17.5	17	17	3.8	3.8	3.8	3.8	4.7368	-13.013
2	14.5	13.5	14	14	3.8	3.8	3.8	3.8	3.6842	-11.327
3	9.8	9.9	10	9.9	3.8	3.8	3.8	3.8	2.605	-8.317
4	10.7	10.2	10.5	10.5	3.1	3.7	3.2	3.33	3.153	-9.975
5	12.55	12.75	12.5	12.6	3.8	3.8	3.8	3.8	3.3157	-10.411
6	14.5	14	15	14.5	3.8	3.8	3.8	3.8	3.8157	-11.631
7	11.6	12	12	11.8	2.7	2.5	2.6	2.6	4.5384	-13.138
8	9.9	10.1	10	10	1.9	2	1.8	1.9	5.263	-14.425
9	11.2	10.9	10.9	11	1.9	1.3	1.3	1.5	7.3333	-17.306

The microstructure evolution in the CCSMD and PCSMD processes was extensively investigated in this study for understanding the difference in the morphology and microstructure in both processes. Optical microscopy was used to obtain the microphotographs. Cross-sections and side wall specimens were prepared for metallographic testes using the standard procedures reported in metal handbook (1975). All specimens were electro-etched using 10gr oxalic acid with 100 ml distilled water at 9 V for 30-60 S.

Transverse tensile tests were carried out on the subsize sheet specimens prepared according to ASTM: E8/8M standard (ASTM standard, 2011) with a gauge length of 25 mm, and cross-section within the gauge length of 6.25x3.8 mm². Tests were performed using testing machine with displacement rate of 1 mm.min⁻¹. Three trial of experiments were performed for assessing the tensile properties of the weldments.

The sets of process parameters used in this work used for investigating the effects on the microstructure characteristics and tensile properties are summarized in Table 5.

Table 5 Welding conditions used for preparing tests specimens of butt joint weldments

Welding process	Exp. No.	Cooling state (Cs)	Travel speed TS (mm/s)	Wire feed speed WFS (m/min)	Frequency F (Hz)	Peak tempertue °C	Cooling rate °C/second	Heat input Hi J/mm
CC TW	A	0	1	0	0	1046.45	7.12	1815.6
	B	2	3	2	0	1044	29	605.2
PCTW Low frequency	C	0	3	4	5	1028	13.23	454
	D	2	2	0	5	829	24	681
PCTW High frequency	E	0	2	2	500	986.5	8	681
	F	2	1	4	500	919	13.6	1361.7

3. Results and Discussions

3.1 S/N Ratios of Aspect Ratio Analysis and Main Effects Plot

The various bead profiles and depth of penetration for all the L9 experiments were shown in Figure 3 and Table 6. The aspect ratio was calculated experimentally and taguchi method was used for analysis together with aid of analysis of variance. The main effects plots for the S/N ratios are shown in Fig. 4, which shows that the S/N values decrease with increasing the TS, WFS, and F, but S/N values increase with increasig the cooling rate. The optimal process parameters have been established by analyzing response curves of S/N ratio. From Fig. 4, it is concluded that the third level of travel speed (3 mm/s), third level of wire feed rate (4 m/min), third level of frequency (500 Hz) and first level of cooling state (low cooling rate) give the optimal aspect ratio. Analysis of variance of S/N ratio is summarized in Table 7. It is obvious that the travel speed is the most important factor affects aspect ratio with maximum percent attribution of 43 % followed by cooling rate with percent attribution of 19 % and no contribution for the frequency.

The response values for S/N ratio for each level of identified factors have been listed in Table 8, which shows the factor level values of each factor and their ranking

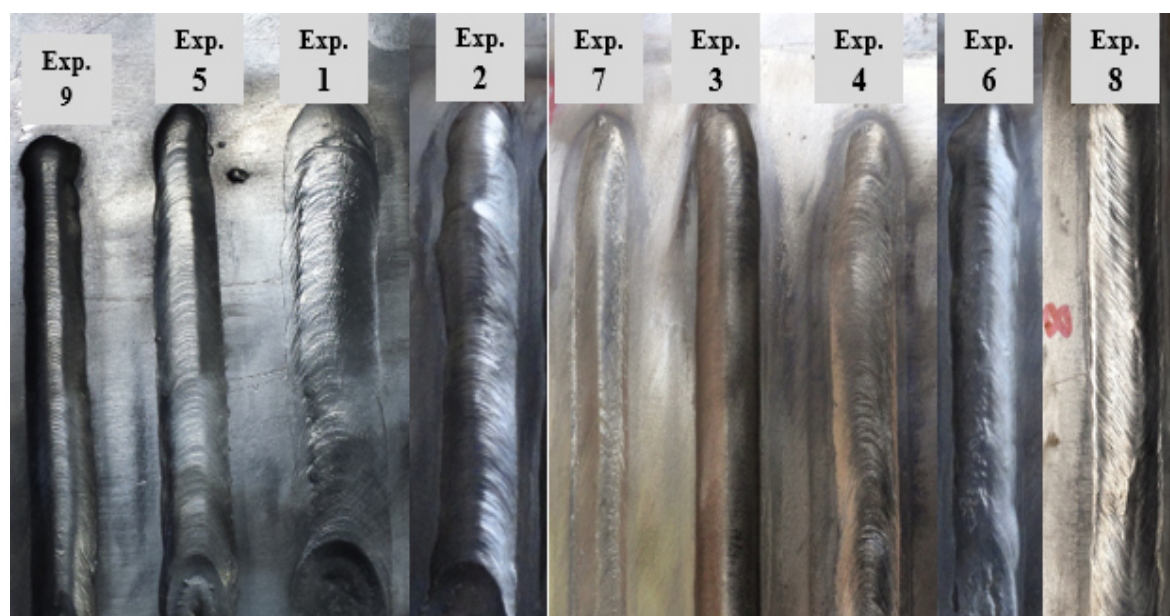
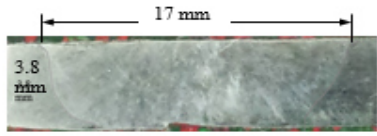
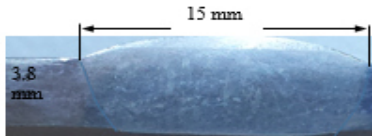
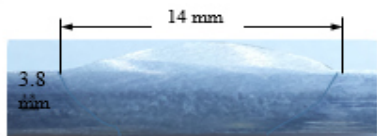
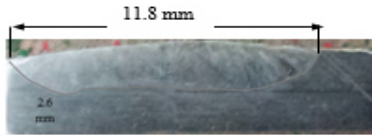
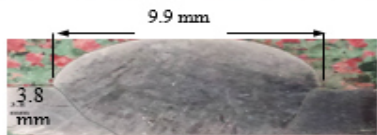
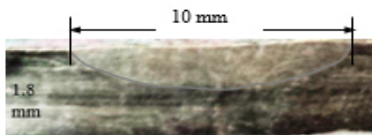
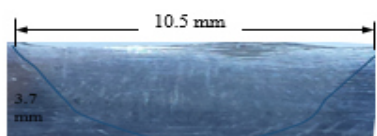
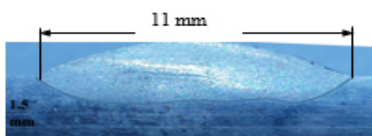
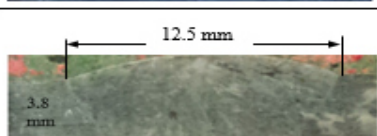


Figure 3 Photographs illustrate the bead on plate profile of the L9 experiments

Table. 6 Photographs illustrate the depth of penetration and bead width

Exp No.	Profile	Exp No.	Profile
1		6	
2		7	
3		8	
4		9	
5			

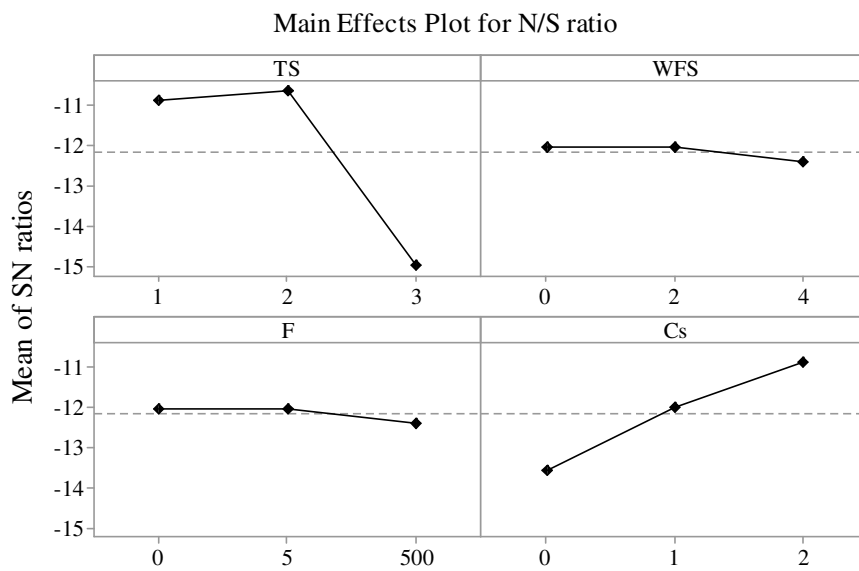


Figure 4 Main effects plot for S/N ratios of aspect ratio

Table 7 ANOVA for means of UTS

Source	DOF	Seq. SS	Adj. MS	F-value	P-value	Percent contribution
TS	1	24.8555	24.8555	4.73	0.309	43.71%
WFS	1	0.2121	0.0001	0.00	0.095	0.37%
F	1	0.0617	0.0617	0.01	0.997	0.11%
Cs	1	10.7014	10.7014	2.03	0.919	18.82%
Error	4	21.0394	21.0394			37.00%
Total	8	56.8701				
R-Sq. = 63%						

Table 8 Response table for S/N ratios of AR for smaller the better characteristic

level	TS	WFS	F	Cs
1	-11	-12.1	-12.1	-13.7
2	-10.75	-12.25	-12.2	-12.2
3	-15	-12.4	-12.6	-11
delta	4.25	0.3	0.5	2.7
Rank	3	3	3	1

3.2 Microstructure and Tension Characteristics

Using the welding conditions reported in Table 5 for preparing welded specimens of similar AISI 304L plates. The heating and cooling curves for all experiments are shown in Figure 5. The peak temperature values are listed in Table 5. The cooling rate was calculated for temperature drop from peak to 300 °C.

From the microstructure results, it is clear that two different kinds of δ -ferrite, namely lathy and skeletal δ -ferrite are formed in the austenitic matrix. Figure 6 shows the variation of δ -ferrite morphology in weld zone using CCTGA of experiments A and B. Experiment A shows the microstructure of specimen prepared without using the copper strip and without adding filler metal, whereas experiment B shows the effects of using continuous water cooling system and with adding filler metal. Fig. 6a depicts greater skeletal and vermicular δ -ferrite with high grain size, and Figure 6b reveals that the grain size generally was finer and higher concentration of total δ -ferrite content compared to experiment A (Figure 6a). The changes in microstructure associated with the amount of heat input to weld pool during the deposition process according to the Eq. (2) (Kou, 2003).

$$H_i \left(\frac{J}{mm} \right) = \eta I \frac{V_{av}}{TS} \quad (2)$$

where H_i is the heat input per unit length; η is arc efficiency (assumed to be 0.83) for TIG welding (Kou, 2003), V_{av} : the average of the instantaneous arc voltage.

In PCSMD process, the heat input can be calculated using the Eq. (2) but here the welding current is I_{av} as shown in Eq. (3) (Giridharan and Murugan, 2009) and the average peak current for pulsed current can be calculated using Eq. (4) (Farhani et al, 2014).

$$H_i \left(\frac{J}{mm} \right) = \eta I_{av} \frac{V_{av}}{TS} \quad (3)$$

$$I_a = \frac{I_p t_p + I_b t_b}{t_p + t_b} \quad (4)$$

where I_{av} the average current for pulse current TIG welding, t_p is the peak time (s) and t_b is the base current duration (s), I_p is the peak current and I_b is the base current

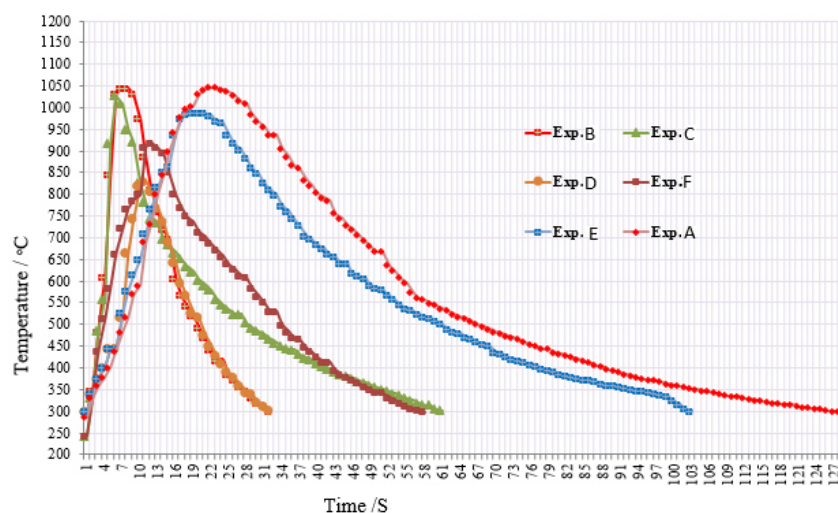


Figure 5 Plots illustrate the heating and cooling curves

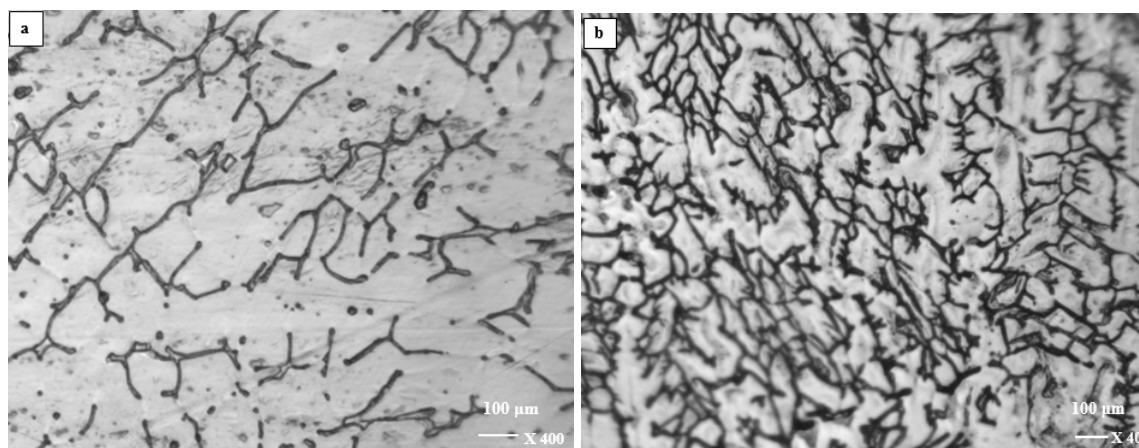


Figure 6 CCTIG (a) exp. A (TS 1mm/s, WFS 0, Cs 0) and (b) exp. B (TS 3mm/s, WFS 4m/min, Cs 2). Showing the existing of long dendrites arms and continuous network of residual ferrite.

The amount of δ -ferrite exists in the weld metal depends on several factors, the most significant factors are chemical composition of the filler and base metal, welding procedure, and the amount of heat input to the melting pool during the welding process (Eglimi et al, 2013). Furthermore, the process of rapid solidification with high temperature gradient, it is beneficial to obtain fine microstructure. Low heat input to the weld zone may result from high travel speed, using continuous cooling system, or using high pulse frequency. Figure 7 shows the effects of pulse frequency on the microstructure texture. High frequency leads to break the dendritic arm of the austenitic stainless steels and produces uniform structure (see Fig.7b). Mourad and others (2012) demonstrated that residual ferrite is strongly influence by the heat input. At high cooling rates, which result from pulsed current process, high travel speed, or continuous water cooling system the transformation of δ -ferrite to austenite is suppressed and higher residual ferrite content in the welding metal is expected as shown in Figures 6b and 7b. Figure 8 describes the effects of the pulsed current on columnar grains as comparing to conventional current process. It is obvious that the pulse frequency significantly affects the dendries arms of the solidified structure at the weld metal and hence it influences the tensile properties welded parts. The tensile test results are summarized in Figure 9. It is obvious that the high ultimate strength was achieved at high frequency (500 Hz) and continous water cooling conditions as shown in exp. F (Figure 9a), also at low frequency (5Hz) and continuous water cooling state (see exp. D in Figure 9a). The ultimate strength is also improved using continuous water cooling staoute in the CCTW process see exp. B in Figure 9a. On other hand, the ultimate strength reduced to minimum value in exp. C, this may be attributed to the low amount of heat input (454 J/mm) with high wire

feed rate (4 m/min) and so insufficient melting of the filler and incomplet fusion occurred.

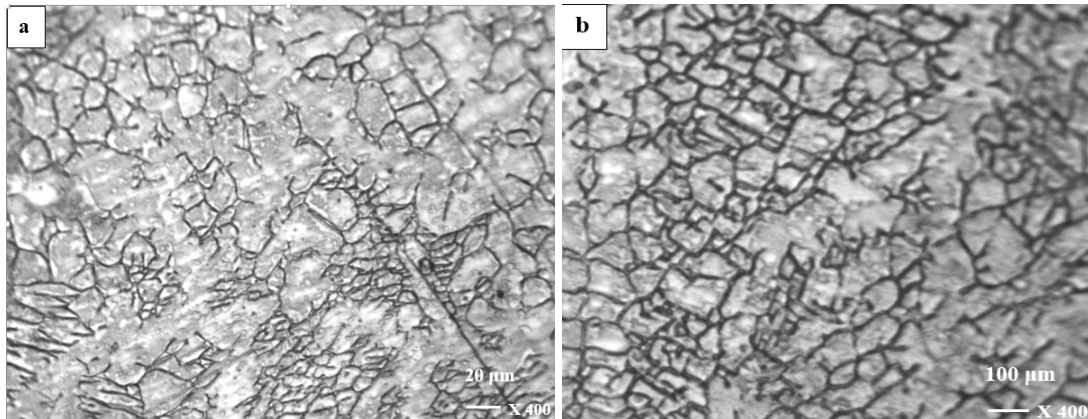


Figure 7 PCTIG (a)exp. 3 (TS 1 mm/s, WFS 4 m/min, Cs 2, F 5 Hz), (b) exp. 7 (TS 3 mm/s, WFS 0 m/min, Cs 1, F 500 Hz), showing the stopping of dendritic arms and uniform structure with fine grains and high residual ferrite.

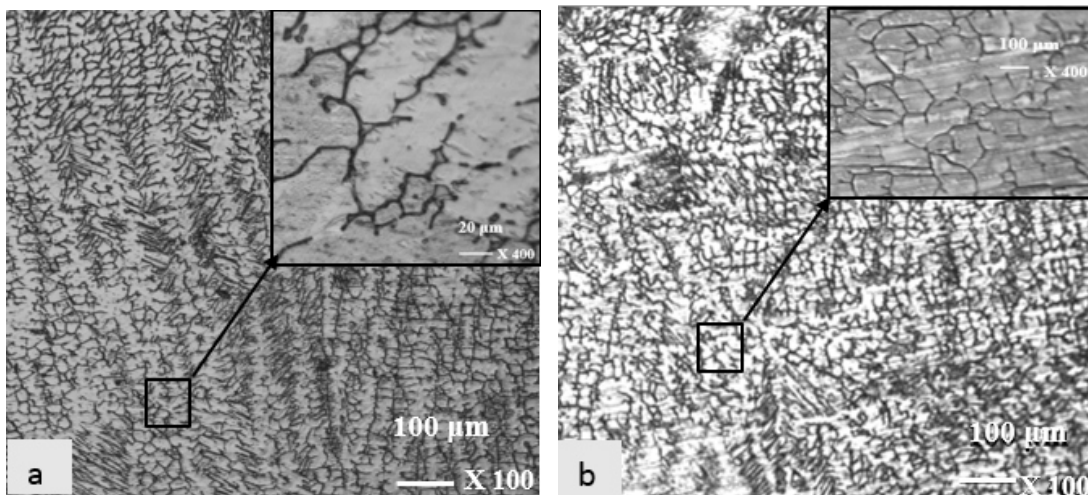


Figure 8 Micrographs illustrate the effects of frequency on the dendritic arms (a) continuous current (exp. A) and (b) pulsed current (exp. E).

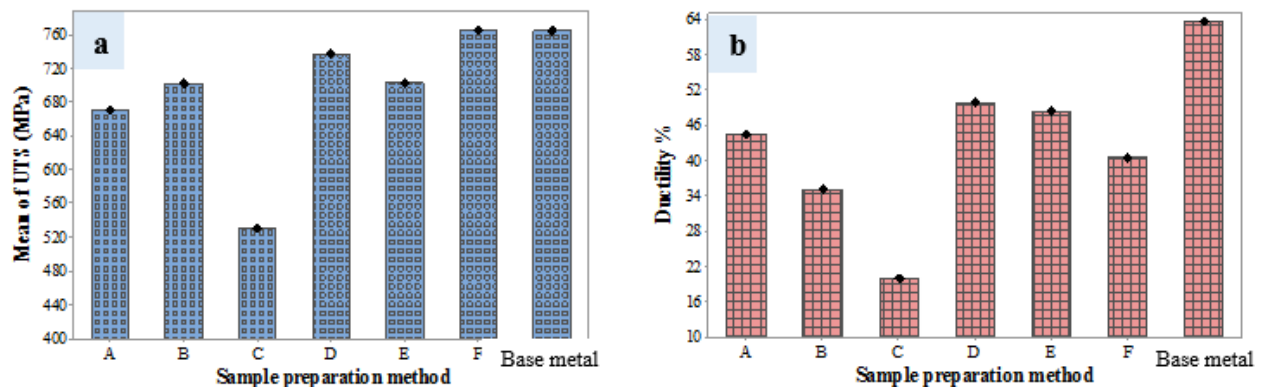


Figure 9 Plots illustrate the (a) ultimate tensile strength, and (b) ductility % which are measured for different sets of welding process parameters.

4. Conclusion

This paper has presented the optimization of welding process parameters using 3.8 mm sheets of AISI 304L stainless steel material through experimental study for non-pulsed & pulsed current TIG welding. The L9 orthogonal array has been used to assign the selected parameters and using the analysis of variance to analyze the results. The main outcomes of this work have been deduced as concluding summary as follows:

1. The results show that the travel speed is the most significant factor influences the aspect ratio with contribution percent of 43% followed by cooling state with contribution percent of 19 %.
2. Optimal aspect ratio can be achieved through using PCTW process with the following optimal values of welding conditions: TS 3mm/s, WFS m/min, F 500 Hz, and low cooling rate system.
3. High pulse frequency significantly affects on the morphology of the welded parts and hence improves the mechanical properties. Since it significantly affects the grain size through breaking the dendrite arms as well as the amount of δ -ferrite is relatively higher. Whereas, the cooling state factor also influences on the tensile strength, since it creates a fine structure with high residual δ -ferrite content which leads to improve the properties of the weldments.
4. The highest tensile strength achieved during this research is 765.8 MPa achieved at frequency of 500 Hz and using continuous water cooling system. Which is comparable to the base metal and superior to the conventional process.
5. There is no evidence of any sensitization of the welded parts can be seen for all specimens also no other defects can be observed in all cases during macro- and microstructure tests.

References

- A Eghlimi, M. Shamanian, and K. Raeissi, (2013) "Dilution and ferrite number prediction in pulsed current cladding of super-duplex stainless steel using RSM," *Journal of Materials Engineering and Performance* 22(12), 3657-3664.
- A.H.I Mourad, A. Khourshid, and T. Sharif, (2012) "Gas tungsten arc and laser beam welding processes effects on duplex stainless steel 2205 properties", *Materials Science and Engineering, A* 549, 105-113.
- A. Namjou, R. Dehmlaei, A. Sharafi, (2014) "A Comparative study," in Magnetism, vol. III, on direct pulsed current gas tungsten arc welding of 25Cr-35Ni heat resistant steel", *International Journal of Natural and Engineering Science* 8(11), 22-28.
- Arivarasu M., Devendranath Ramkumar K, Arivazhagan N., (2014) "Comparative studies of high and low frequency pulsing on the aspect ratio of weld bead in gas tungsten arc welded AISI 304L plates", *Procedia Engineering* 97, 871-880.
- ASTM International. Standard test methods for tension testing of metallic materials [metric]. Standard E8/E8M-09, *ASTM International, W. Conshohocken, Pa*, 2011.
- Balasubramanian, B., Jayabalan, V., Balasubramanian, V., (2006) "Optimizing the pulsed current gas tungsten arc welding parameters", *Journal of Materials Science and Technology* 22(6) 821-825.
- Sadek, C., Alfaro, A., Chawla, K.S., Norrosh, J., (1995) "Computer based data acquisition for welding research and production", *Journal of Materials Processing Technology* 53, 1-13.
- Farahani, E., Shamanian, M., Ashrafizadeh, F., (2012) "A comparative study on direct and pulsed current gas tungsten arc welding of alloy 617", *International Journal on Manufacturing and Material Science* 2, 1-6. doi: 01IJMMMS.0201.41.
- Giridharan, P.K., Murugan, N., (2009) "Optimization of pulsed GTA welding process parameters for the welding of AISI 304L stainless steel sheets", *International Journal of Advanced Manufacturing Technology* 40, 478-489. doi: 10.1007/s00170-008-1373-0.
- Mao, J., Lü, W., Wang, L., Zhang, D., Qin, J., (2014) "Microstructure and mechanical properties of GTA weldments of titanium matrix composites prepared with or without current pulsing", *Journal of Transaction of Nonferrous Metals Society China* 24, 1393-1399.
- Ramkumar, K. D., Choudhary, A., Aggarwal, S., Srivastava, A., (2015) "Characterization of microstructure and mechanical properties of continuous and pulsed current gas tungsten arc welded superaustenitic stainless steel", *Journal of Materials Research* 30(10), 1727-1746.
- Kou, S., (2003) "Welding Metallurgy. 2nd Edition, John Wiley & Sons, INC.
- Prasad, K. S., Rao, C. S., Rao, D.N., (2012) "An investigation on weld quality characteristics of pulsed current micro plasma arc welded austenitic stainless steels", *International Journal of Engineering Science Technol* 4(2), 159-168.

- Metals Handbook, (1973) Metallographic, structures and phase diagrams. 8th Edition, American Society for Metals, Metal Park, Ohio 44073 USA.
- Hamjah, M. K. B., (2014) "Optimization of new semi-automatic TIG welding process for surface quality through Taguchi method," *PhD Thesis*, University of Tun Hussein Onn, Malisia.
- Yousefieh, M., Shamanian, M., Saatchi, A., (2011) "Optimization of the pulsed current gas tungsten arc welding (PCGTAW) parameters for corrosion resistance of superduplex stainless steel (UNSS322760) welds using the Taguchi method", *Journal of Alloys and Compounds* 209, 782-790.
- Dinesh Kumar, R., Elangovan, S., Siva Shanmugam, N., (2014) "Parametric optimization of pulsed-TIG welding process in butt joining of 304L austenitic stainless steel sheets", *International Journal of Engineering Research and Technology* 3(11) 213-219.

Adnan A. Uglu (adnanugla76@gmail.com) is currently Assistant Professor in advanced manufacturing processes, College of Engineering, Thi-Qar University in Al-Nasiriyah /Iraq. He is member of Advanced Manufacturing Technology Research Group and his research interests mainly cover additive manufacturing, welding based shaped metal deposition, welding processes and quality control. He has published journal papers and participated some of International conferences in the same area.